Journal of Applied Polymer Science

Low Temperature One-Step Synthesis of Poly(barbituric acid) Functionalized Magnetic Nanoparticles for Removal of Heavy Metal Ions

Shi Lan, Ruiqing Li, Zhihua Leng, Na Guo, Shucai Gan
College of Chemistry, Jilin University, Changchun 130026, People's Republic of China
Correspondence to: S. Gan (E-mail: gansc@jlu.edu.cn)

ABSTRACT: Poly(barbituric acid) functionalized magnetic nanoparticles with excellent adsorption behavior were facilely synthesized through one-step chemical oxidation polymerization method by using sodium borohydride as the reducing agent. Structure, morphology, and magnetism of the products were thoroughly investigated by means of FTIR, FESEM, EDX, X-ray photoelectron spectra, thermogravimetric analyzer–differential scanning calorimetry, and vibrating sample magnetometer. The products were of a sphere-shaped nanostructure with the saturation magnetization value of 7.5 emu g^{-1}, which make them reusable for adsorption application. Removal capability for heavy metal ions were systematically evaluated using Pd (II) and Cu (II) ions as the models. The maximum sorption capacities by applying the Langmuir equation were calculated to be 166.6 mg/g for Cu (II) and 142.8 mg/g for Pb (II). A recycle test revealed that the PBA-MNPs have above 87.1% for Cu (II) and 82.69% for Pb (II) ion desorption efficiency after the three regeneration cycle process. All the above experimental results demonstrated that barbituric acid-based material could be used as a possible adsorbent for the efficient removal of heavy metals from aqueous solution. © 2014 Wiley Periodicals, Inc. J. Appl. Polym. Sci. **2014**, *131*, 40957.

KEYWORDS: adsorption; applications; magnetism and magnetic properties

Received 19 February 2014; accepted 4 May 2014
DOI: 10.1002/app.40957

INTRODUCTION

Barbituric acid (BA) is a promising heterocyclic compound with two imide functional groups in the structure.[1] Recent considerable research efforts have been devoted to study its pharmaceutical and biological effect.[2] Nevertheless, this is the first report about the adsorption behavior of BA toward pollutants. It can be expected as a promising candidate for efficient adsorbent of heavy metal ions because the BA has ample metal-binding atoms with strong affinity for heavy metal ions. The occurrence of heavy metals especially copper and lead in industrial and ground effluents brings serious environmental pollution, threatening human being, animals, and plants. Lead is considered to be one of the most toxic heavy metals often found in a wide variety of industrial process, such as glass industries, petroleum refining, and battery manufacture, etc.[3–5] Copper contaminants usually present in refinery rigs or fuel-handing systems.[6,7] These heavy metals exceeding permissible limits can cause various diseases in daily life, e.g. headache, nausea, coryza, pharyngitis, emphysema, and lung cancer.[8–10] Therefore, controlling heavy metal contamination is an important issues. However, there is a major drawback for the application of BA as an adsorbent originating from the separation due to its recovery problem deriving from solubility in aqueous solution. Hence, it is anticipated that coating of magnetic nanoparticles with BA can make these adsorbents recoverable conveniently. Recently, many studies have been performed to incorporate the metal-binding functional groups, e.g. carbonyl and amino groups, on the surface of iron oxide nanoparticles, which can not only enhance heavy metal ions uptake but also efficiently separate adsorbent under an external magnetic field.

Up to date, much research efforts have been directed toward the synthesis of magnetic hybrid particles.[11] Recently, a series of polymer hybrid materials have been prepared including magnetic-poly(divinylbenzene)-poly(*N*-isopropylacrylamide-*co*-acrylic acid),[12] magnetic poly(*N*-isopropylacrylamide),[13] magnetite chitosan,[14] aminodextran coated-magnetic poly(divinylbenzene) nanoparticles,[15] Fe_3O_4-Am-*N*, *N*′-methylene bis (acrylamide) (MBA),[16] magnetic polyaniline,[17] polystyrene/γ-Fe_2O_3,[18] polyrhodanine-encapsulated magnetic nanoparticles (PR-MNPs),[19] γ-Fe_2O_3-P (glycidyl methacrylate (GMA)-ethylene glycol dimethacrylate (EGDMA)),[20] Fe_3O_4-SiO_2-Poly(allylamine)-perfluorophenyl azides (PAA-PFDA),[21] and Fe_3O_4-P(methyl methacrylate-divinylbenzene (MMA-DVB)),[22] etc. Polymer encapsulation can not only provide surface functionalization but also protect the magnetic

nanoparticles from aggregation to increase their stability. The synergism between magnetism and adsorption may be a promising candidate for both fundamental research and functional applications.

In the present work, poly(BA) functionalized magnetic nanoparticles were facilely synthesized through one-step chemical oxidation polymerization technique. The as-synthesized magnetic functional particles have high sorption capacity for Cu (II) and Pb (II) ions. In addition, the magnetic property of PBA-MNPs provides the recyclable application in the wastewater treatment. Experimental results indicated that BA is a promising candidate for efficient adsorbent of heavy metal contaminants.

EXPERIMENTAL

Materials

BA was purchased from Tianjin Chemical Reagent Research Company. Ferric chloride hexahydrate ($FeCl_3{\cdot}6H_2O$) and sodium borohydride ($NaBH_4$) were purchased from Beijing Chemical Reagent Research Company and used without further purification. For batch adsorption experiments, Copper nitrate ($Cu(NO_3)_2{\cdot}3H_2O$) and lead nitrate ($Pb(NO_3)_2$) were purchased from Shanghai Chemical Reagent Plant. Distilled water was used in all experiments.

Characterization

The infrared spectra of the nanocomposites was taken in KBr pressed pellets on a NEXUS 670 infrared Fourier transform spectrometer (Nicolet Thermo, Waltham, MA). Scanning electron microscopy (SEM) was performed on a TESCAN 5136MMSEM at an accelerating voltage of 20 kV. The samples were loaded onto a Si substrate previously sputter coated with a homogenous gold layer for charge dissipation during the SEM imaging. X-ray photoelectron spectra (XPS) measurement was carried out on a PHI-5000CESCA system with Mg K radiation ($hv = 1253.6$ eV). The X-ray anode was run at 250 W, and the high voltage was kept at 14.0 kV with a detection angle at 540. All the binding energies were calibrated using the containment carbon. Differential scanning calorimetry–thermogravimetric analyzer (DSC/TGA 1600 LF, METTLER TOLEDO, Switzerland) up to 800°C was performed on the sample at a heating rate of 10°C min^{-1} while N_2 gas flow rate of 60 mL min^{-1}. The hysteresis loops were obtained with a vibrating sample magnetometer (VSM 7407, Lake Shore). The surface analysis–zeta potential measurement was performed by Brookhaven Instruments Corporation–ZetaPlus.

Synthesis of Poly(barbituric acid) Functionalized MNPs

The PBA-MNPs were synthesized by one-step chemical oxidation polymerization method.[23] The details were described as follows. Initially, BA monomers (0.82 g, 5 m*M*) were dissolved in 100 mL deionized water and the above solution was heated continuously to 83°C with vigorous mechanical stirring. After mechanical stirred for 30 min, an aqueous solution of iron chloride (1.35 g, 5 m*M*) was injected to obtain a stable solution and followed by the addition of 15 mL sodium borohydride solution (0.569 g) under mechanical stirring, and the process was followed for 20 h. Finally, the brown product was collected with the help of external magnet, then washed and vacuum-dried for further characterization.

Adsorption Experiments

The as-synthesized PBA-MNPs can be used as potential adsorbents for the removal of heavy metal ions owing to their high surface area, ample active sites, and superparamagnetism. Heavy metals such as copper and lead were selected in this study because they were the most toxic metal contaminants to humans and all living systems. A stock solution (1000 mg/L) of metal ions was prepared by dissolving copper nitrate and lead nitrate in deionized water. Solution with the desired initial concentrations (Cu (II) and Pb (II): 50–300 mg/L) were obtained by successive dilutions. Batch adsorption experiments were carried out at 30°C in thermostat water bath under an agitation speed of 150 rpm. After the adsorption equilibration was achieved, the adsorbents were separated with the help of external magnetic field and the residual target ions concentration in the clear solution were calculated by flame atomic absorption spectroscopy (FAAS). The heavy metal ions concentration before and after adsorption were detected to determine the relative adsorption capacity and removal efficiency. For accurate adsorption results, the responding adsorption date were analyzed three times and the results were averaged. The adsorption capacity (q_e) and the adsorptivity (R) were calculated using the equations as follows[24]:

$$q_e = \frac{(C_0 - C_e) \times V}{W}$$

$$R = \frac{C_0 - C_e}{C_0}$$

where C_0 is the initial concentration of metal ions (mg/L), C_e is the equilibrium concentration of metal ions after adsorption (mg/L), V is the volume of metal ions solution (mL), and W is the weight of the synthesized adsorbent (mg).

RESULTS AND DISCUSSION

Fabrication and Characterization of PBA-MNPs

The schematic illustration of the fabrication process of poly(BA) functionalized magnetic nanoparticles is illustrated in Figure 1(a). Initially, the iron chloride was added into the BA aqueous solution, and the metal-binding functional groups of BA monomer coordinated with Fe ions. The solution color changed to black, this indicates that the iron hydroxide form at the initial stage of reaction. When sodium borohydride solution was added, the solution color changed from black to brown and generated a lot of bubble, which indicates the iron ions became magnetic Fe_2O_3 MNPs through oxidation–reduction reaction. Finally, the iron ions resulting from the surface oxidation of magnetic Fe_2O_3 MNPs nanoparticles triggered the oxidation of BA monomer to obtain PBA-MNPs via oxidation polymerization. The chemical oxidation polymerization mechanism of the BA is shown in Figure 1(b). Based on the previous study, the iron ions formed on the surface of Fe_2O_3 MNPs accept the electron from BA monomer and trigger the polymerization of BA.[19,25,26]

Results of SEM, fourier transform infrared spectroscopy (FTIR), and energy dispersive X-ray spectrum (EDX) analysis of PBA-MNPs composite are displayed in Figure 2. Typical SEM image in Figure 2(a) depicts the spherical shape and relatively rough

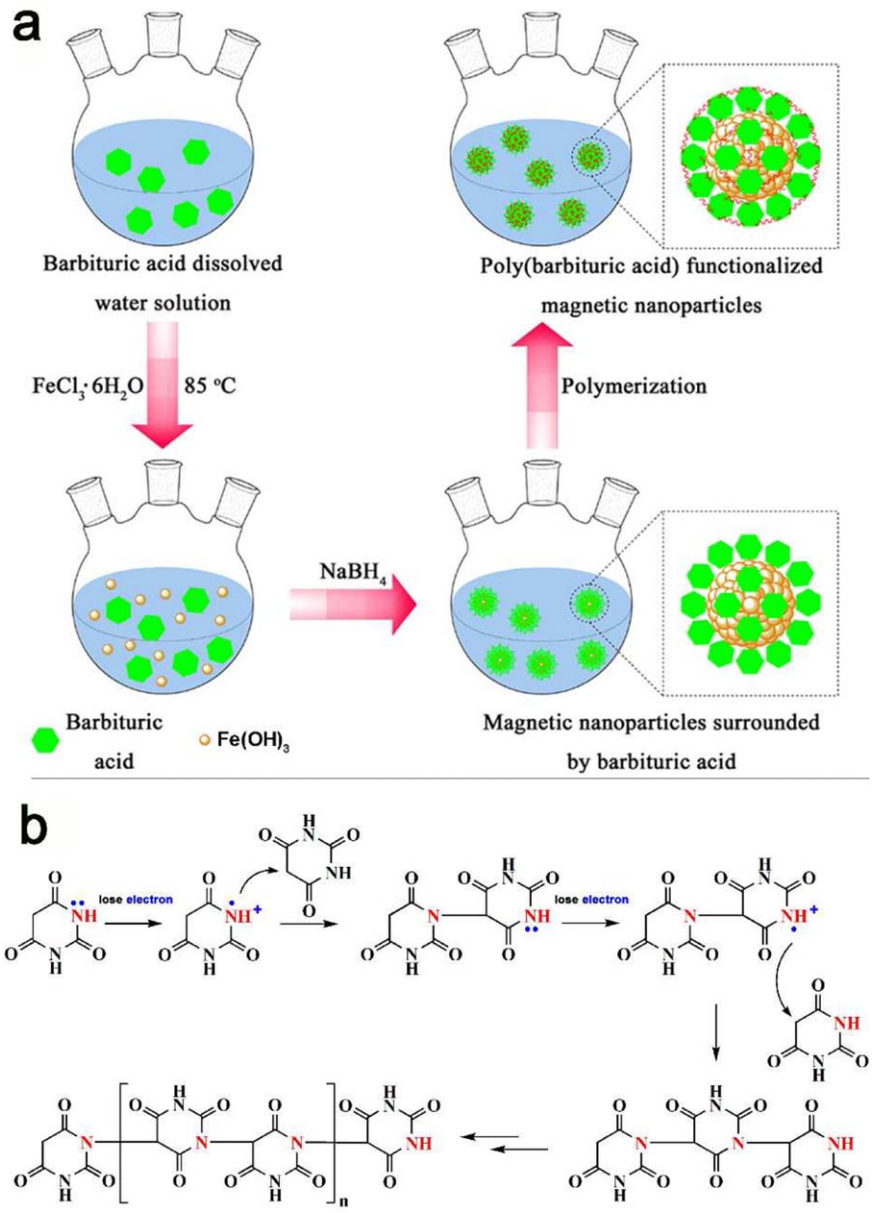

Figure 1. Schematic illustration of the fabrication process of poly(BA) functionalized magnetic nanoparticles (a), chemical oxidation polymerization mechanism of the BA (b). [Color figure can be viewed in the online issue, which is available at wileyonlinelibrary.com.]

surface of PBA-MNPs nanoarchitecture. These spherical functional particles were formed by smaller spherical agglomerates of dimension ~15 nm. It is attributed to the fact that the metal-binding groups coordinate with the iron ions, and then limit core nanoparticles to grow bigger. The size distribution histogram is shown in inset Figure 2(a). The size distribution of the PBA-MNPs was reasonably narrow, and the average particle size was determined as 327 nm. The magnetic functional nanocomposites maintain a distributed uniform state to some extent. FTIR was recorded to confirm the formation of PBA-MNPs as well. As shown in the Figure 2(b), the broad characteristic band centered around 3367 cm^{-1} corresponds to the stretching vibration of hydroxy group. Moreover, besides Fe—O bond from Fe_2O_3 located at 630 cm^{-1} and 578 cm^{-1}, peaks at around 2872, 1710, 1053, 1421, and 785 cm^{-1} were attributed to the stretching vibrations of C—H, C═O, C—N, C—O and out-of-plane bending of C—H bond from BA unit, demonstrating the successful preparation of PBA-MNPs.[27–29] The EDX map of PBA-MNPs was monitored to further confirm the formation of PBA-MNPs in Figure 2(c). EDX analysis clearly showed the existence of Fe, O, C, and N elements, confirming the successful fabrication of magnetic functional composite. Moreover, elemental Si observed in the EDX spectra was derived from the Si substrate and the Au peak corresponded to Au deposited on the tested sample before measurement. The SEM, FTIR, and EDX result adequately verified the product in morphology and structure.

The chemical bonding states in PBA-MNPs composite were analyzed by XPS measurement, and the corresponding results are shown in Figure 3. The X-ray photoelectron spectrum

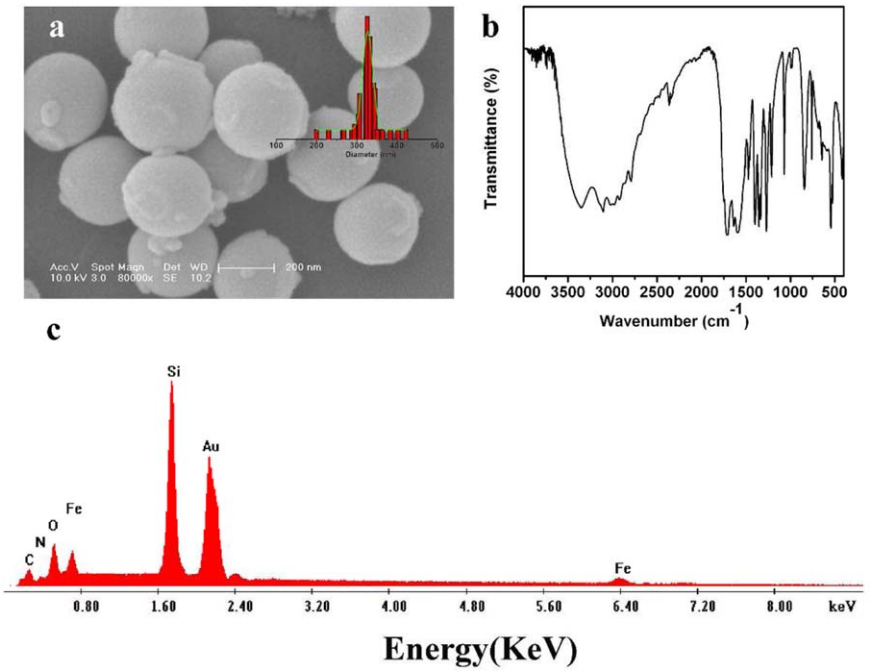

Figure 2. (a) SEM image and particle size distribution (the inset in a), (b) FTIR spectra, and (c) EDX map of the PBA-MNPs composite. [Color figure can be viewed in the online issue, which is available at wileyonlinelibrary.com.]

survey of PBA-MNPs composite particles [Figure 3(a)] displayed peaks at Fe 3p (57.5 eV), C 1s (284.6 eV), O 1s (532.0 eV), and N 1s (402.9 eV) corresponding to the Fe_2O_3, C—C, C═O, and —-NH_2, showing the successful combination of Fe_2O_3 with BA-based polymer.[26,30] The chemical bonds of PBA-MNPs composite were further illustrated from the magnified Fe 2p, C 1s, O 1s, and N 1s peaks. As shown in Figure 3(b), the photoelectron peak of Fe $2p_{1/2}$ and Fe $2p_{3/2}$ was detected at 711 eV and 723 eV, which matched closely with that of standard Fe_2O_3 recorded in the literature.[31] The C 1s peak [Figure 3(c)] was curved into three peak components, which were attributed to the C—C, C—N, and C═O groups, respectively.[32] In Figure 3(d), the curve fitting of O 1s revealed three separate peaks corresponding to Fe—O, Fe—OH, and C═O bond, respectively.[33,34] The N 1s peak observed in Figure 3(e) reflected the existence of CONH bond in PBA-MNPs composite.[35] The Fe 2p, C 1s, O 1s, and N 1s spectrum not only exhibit the surface chemistry and but also further verify the successful formation of PBA-MNPs composite.

The thermal stability of the PBA-MNPs and pure BA was measured by thermogravimetric analysis. The results are shown in Figure 4. For the PBA-MNPs, the 43.2% weight loss percentage was observed in the range of 275–600°C, which corresponds to the carbonized BA [Figure 4(a)]. Moreover, the weight loss curve kept platform and the weight residue of 46.7% appeared at 600°C, which is attributed to the magnetic materials and decomposition of residual organic compound. It should be noted that the weight changes of pure BA are nearly completed at about 800°C. As shown in Figure 4(b), the initial steep change region between 200°C and 300°C can be ascribed to the loss of residual water adsorbed physically in the sample and the degradation of oxygen-containing groups.[36]

The magnetization hysteresis loops of the PBA-MNPs and pure Fe_2O_3 MNPs prepared under the same reaction conditions were detected by vibrating sample magnetometer (VSM). The results in Figure 5 revealed that PBA-MNPs and Fe_2O_3 MNPs are super-paramagnetic at room temperature.[37] From Figure 5 it can be seen that the measured saturation magnetization (M_s) and coercivity (H_c) for PBA-MNPs decrease to 7.5 emu g^{-1} and 56.92 Oe compared to the pure Fe_2O_3 MNPs (27.8 emu g^{-1} and 87.9 Oe), respectively, owing to the existence of PBA. For the PBA-MNPs, there is a decrease in the magnetization, which is related to the decrease in the content of the MNPs in the nanocomposite. The mass radio of Fe_2O_3 MNPs content in PBA-MNPs is calculated from the equation[38–41]:

$$\sigma_{\text{nanocomposite}} = \text{wt}\,\%_{\text{MNPs}} \times \sigma_{\text{MNPs}}$$

where $\sigma_{\text{nanocomposite}}$ is the magnetization of PBA-MNPs and σ_{MNPs} is the magnetization of bare Fe_2O_3 MNPs at 5 kOe and room temperature. The amount of magnetic material is found to be about 26.9 wt % calculated from the saturation magnetization of PBA-MNPs. The magnetic property is significant for magnetic separation of magnetic adsorbent from aqueous solution by a magnetic field within a few seconds (inset in the Figure 5) and which provides recyclable application in the wastewater treatment.

Batch Adsorption Experiments

Effect of pH Value. It is well known that the solution pH value is one of most important parameters affecting the adsorption property due to its influence on the aqueous chemistry and the surface charge of the adsorbent. The effects of pH value on the adsorption of PBA-MNPs toward Cu (II) and Pb (II) ions were studied by varying the pH value from 3 to 7 by adjusting with 0.1*M* HCl or NaOH, and the results are presented in Figure

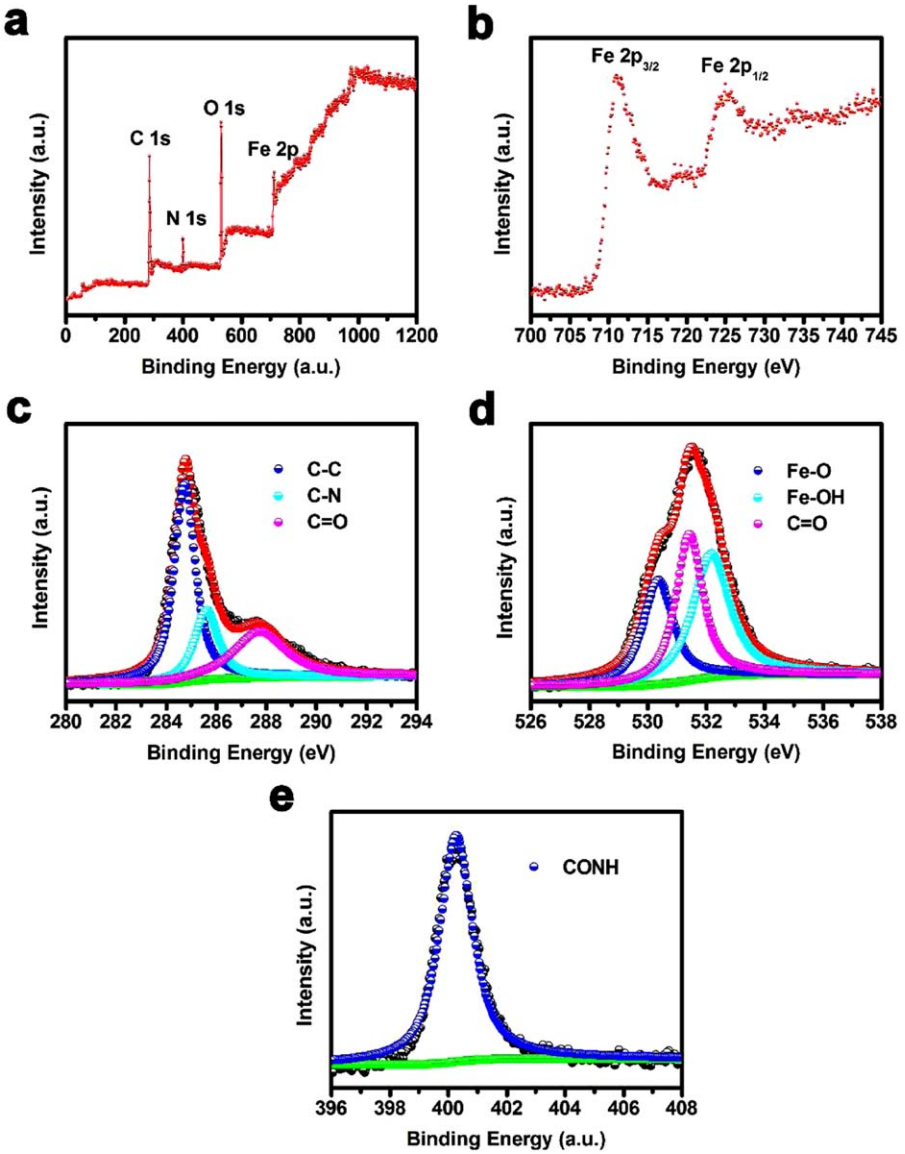

Figure 3. (a) XPS survey spectra of PBA-MNPs. High-resolution XPS spectra of Fe2p (b), C 1s (c), O 1s (d), and N1s (e). [Color figure can be viewed in the online issue, which is available at wileyonlinelibrary.com.]

6(a). It can be seen that the adsorption quantity of Cu (II) and Pb (II) ions increased with increasing the pH value from 3 to 5. As pH value increased to 6, the adsorption capacity was approximately constant. This phenomenon can be stated as follows. When pH value was lower than 3, sorption capacity of metal ions decreased due to the increased competition with H^+ ions for active adsorption sites.[42,43] In acid solution, the as-prepared PBA-MNPs show positive zeta potentials and the positive zeta potentials decrease with increasing the pH value, indicating the surface amino groups became cationic groups in the lower pH value solution. However, the zeta potential decreased and even became negative as the pH increased. This is because the more hydroxyl groups were found on the particle surface with increase in the pH values. The pHzpc (pH value at zero point charge, Figure 6(b) of PBA-MNPs was close to 6.5. Therefore, at pH > pHzpc the surface charge of PBA-MNPs was negative, and the electrostatic interactions between the metal ions and adsorbent become stronger.[44,45] When pH value was higher than 6, a decline in metal ions uptake was observed. It was believed that the solubility of metal ions is also one of the major factors in metal ion removal. Metal ions in water solution can form various speciation at different pH values. The formation of precipitation of metal hydroxides must be taken into account as well.[46,47] In the case of Pb (II) and Cu (II) ions, the slight decrease of adsorption in the range of pH 6–7 can be explained by the formation of hydroxide complexes ($Pb(OH)^+$, $Cu(OH)^+$) due to the equilibrium constants (logK $Pb(OH)^+$ and $Cu(OH)^+$ are -7.46 and -7.95 at 25°C, respectively).[48–50] For Pb (II) and Cu (II) ions, one can calculate that Pb (II) ions are partially hydrolyzed at pH 8.2 and Cu (II) ions at pH 6.4. Accordingly, all experimental pH values were adjusted to 6 for further studies.

Effect of Adsorbent Dosage. The effect of adsorbent dosage on the removal efficiency of PBA-MNPs for Cu (II) and Pb (II)

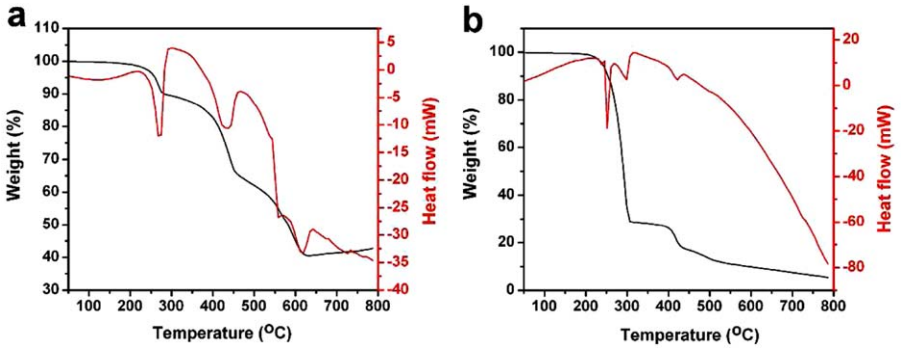

Figure 4. TGA–DSC curves of the PBA-MNPs (a) and the pure BA (b). [Color figure can be viewed in the online issue, which is available at wileyonlinelibrary.com.]

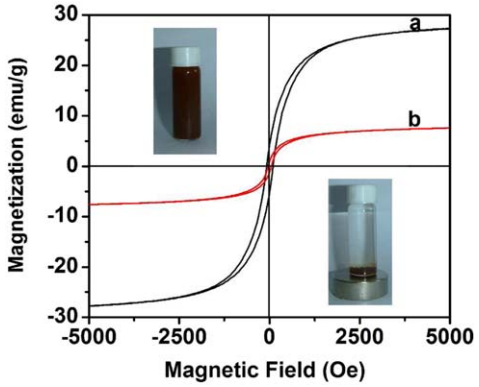

Figure 5. Magnetic hysteresis loops of the Fe_2O_3 MNPs (a) and PBA-MNPs (b) at 298 K and photographs of the PBA-MNPs dispersed in aqueous solution without and with external magnetic field (inset in the Figure 5). [Color figure can be viewed in the online issue, which is available at wileyonlinelibrary.com.]

ions is shown in Figure 7. It can be seen that at a fixed initial concentration of metal ions, the sorption percentage efficiency increased rapidly from 53.6% to 65.2% for Cu (II) and 51% to 62.8% for Pb (II) when PBA-MNPs dose increased from 1 g/L to 2 g/L because that the availability of active surface sites for the adsorption of metal ions increased with an increasing concentration of PBA-MNPs. However, the removal efficiency changed relatively little when the adsorbent weight was beyond 2 g/L. Thus, when the initial concentration of target metal ions was 100 mg/L, the adsorbent weight of 2 g/L was more appropriate. According to HSAB theory, the imide groups of the poly(BA) are regarded as metal-binding groups with strong affinity for heavy metal ions. Thus, the oxygen and nitrogen atoms provide lone electron pair which involved in the chelation between the poly(BA) and heavy metal ions (Figure 8).[51–54]

Effect of Initial Concentration and Adsorption Isotherms Study. Effect of initial concentration on the capacity of heavy metal ions adsorbed onto PBA-MNPs at optimum contact time was studied. The equilibrium isotherm for the sorption of Cu (II) and Pb (II) ions on PBA-MNPs was determined by agitating 100 mg PBA-MNPs with 50 mL of Cu (II) and Pb (II) ions solution of various concentrations. The heavy metal ions uptake performance of the PBA-MNPs was evaluated as a function of the initial metal ions concentration at pH value of 6.0. The adsorption experimental data were analyzed by the typical isotherm models for designing a desired adsorption system. In this study, the Frendlich and Langmuir isotherms are selected to describe the adsorption behaviors of heavy metal ions on PBA-MNPs. The Langmuir model can be expressed by equation[55]:

$$q_e = \frac{K_L q_m c_e}{1 + K_L c_e}$$

The linear form of Langmuir isotherm is as follows:

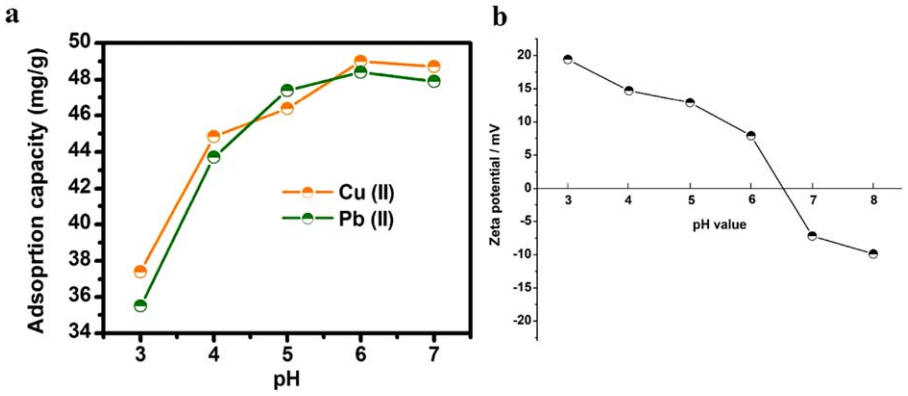

Figure 6. (a) Effect of pH value on the adsorption capacity of PBA-MNPs for Cu (II) and Pb (II) ions. (b) The zeta potential of PBA-MNPs in different pH value solution. [Color figure can be viewed in the online issue, which is available at wileyonlinelibrary.com.]

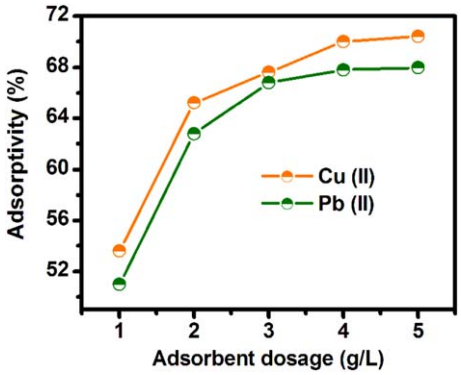

Figure 7. Effect of adsorbent dosage on the adsorptivity of Cu (II) and Pb (II) ions onto the PBA-MNPs. ($T = 30°C$, the concentration of metal ions: 100 mg/L and for 10 h). [Color figure can be viewed in the online issue, which is available at wileyonlinelibrary.com.]

$$c_e/q_e = 1/K_L q_m + c_e/q_m$$

where q_e is the equilibrium adsorption capacity of adsorbent (mg/g), c_e is the equilibrium concentration of metal ions (mg/L), q_m is the maximum amount of metal ions adsorbed (mg/g), and K_L is the constant that refers to the bonding energy of adsorption (L/mg). The Langmuir equation assumes that all the adsorption surface sites with adsorbate affinity do not affect each other so each adsorbate molecule has been located on a single site, and hence it can be considered the monolayer formation of an adsorbate onto the adsorbent surface. On the contrary, the Freundlich model is based on a heterogeneous adsorption. The Freundlich isotherm is given as[55]:

$$q_e = K_F c_e^{1/n}$$

The linear form of Freundlich model can be described as equation:

$$\text{Log } q_e = \text{Log } K_F + \text{Log } c_e/n$$

where q_e is the equilibrium adsorption capacity of the adsorbent (mg/g), c_e is the equilibrium concentration of metal ions (mg/L), K_F is the constant related to the adsorption capacity of the adsorbent (mg/L), and n is the constant related to the adsorption intensity. The relationship between the target ions concentration and the adsorption capacity was analyzed with two different models (Figure 9). The isotherm parameters (K_L, q_m, n, and K_F) and linear correlation coefficient (R^2) values for the typical adsorption isotherm models are shown in Table I. The sorption data were found to obey Langmuir and Freundlich adsorption isotherms but Freundlich isotherm proved to be a better mathematical fit for Cu (II) and Pb (II) ions equilibrium data than Langmuir isotherm, based on the linear correlation coefficient (R^2) values. The maximum sorption capacity q_m (mg/g) of PBA-MNPs by applying the Langmuir equation was found to be 166.6 mg/g for Cu (II) and 142.8 mg/g for Pb (II). In the adsorption isotherm study, the plots of adsorption capacity (q_e) versus the equilibrium concentration (C_e) are shown in Figure 10. As shown in Figure 10, a dotted Freundlich isotherm line fit the experimental data for the sorption of Cu (II) and Pb (II) ions very well. The values of correlation coefficients are all extremely high 0.99.

Effect of Contact Time and Adsorption Kinetics Study. The contact time between the metal ions and the adsorbent was a crucial parameter affecting the removal activity of contaminants from the wastewater via adsorption. The effect of contact time on the amount of Cu (II) and Pb (II) ions adsorbed on the PBA-MNPs was studied at 100 mg/L initial concentration of both metal ions. At various time intervals, adsorbents were taken from the aqueous solution and the concentration of residual target ions in solution was measured. Effects of contact time on the adsorption process were studied with the time ranging from 10 min to 120 min. The kinetic of adsorption process was studied using the pseudo-first-order and pseudo-second-order rate adsorption kinetic models. The pseudo-first-order equation was used as[56]:

$$q_t = q_e(1 - e^{-K_1 t}) \text{ or}$$

$$\ln(q_e - q_t) = \ln q_e - K_1 t$$

where q_t and q_e are the amount of metal ions adsorbed (mg/g) at time t (min) and at equilibrium, respectively, and K_1 is the rate constant of the pseudo-first-order adsorption process (min^{-1}). The straight line plots of $\ln(q_e - q_t)$ against t were used to determine the rate constant K_1 and correlation coefficient R^2 values. The pseudo-second-order model equation is given as[56]:

$$q_t = \frac{q_2^2 K_2 t}{1 + q_2 K_2 t} \text{ or}$$

$$\frac{t}{q_t} = \frac{1}{K_2 q_2^2} + \frac{1}{q_2} t$$

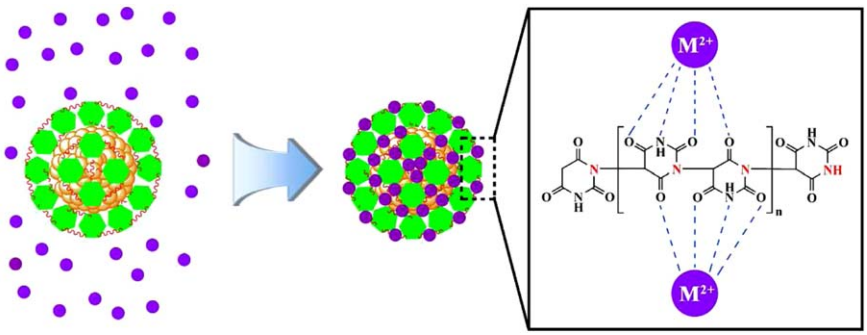

Figure 8. The mechanism for heavy metal ions ($M^{2+} = Cu^{2+}$, Pb^{2+}) adsorption onto PBA-MNPs. [Color figure can be viewed in the online issue, which is available at wileyonlinelibrary.com.]

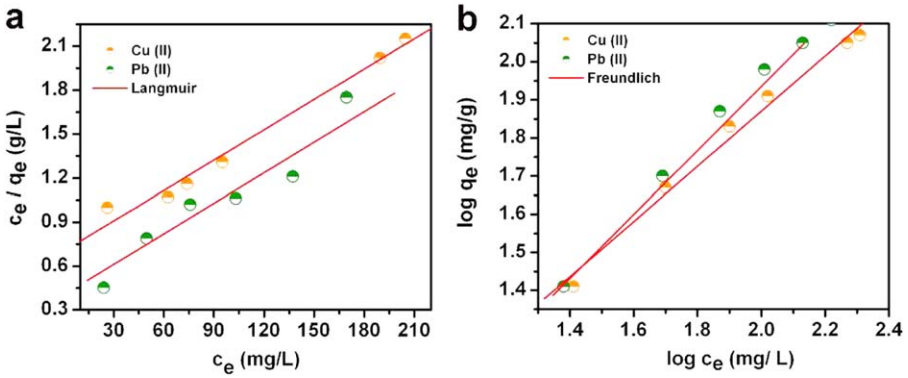

Figure 9. Adsorption isotherm of Cu (II) and Pb (II) ions onto the PBA-MNPs: (a) Langmuir model and (b) Freundlich model. [Color figure can be viewed in the online issue, which is available at wileyonlinelibrary.com.]

Table I. Adsorption Parameters of the Langmuir and Freundlich Models for the Adsorption of Cu (II) and Pb (II) Ions onto the PBA-MNPs

	Langmuir model			Freundlich model		
	q_m (mg/g)	k_L (1/mg)	R^2	K_F	N	R^2
Cu (II)	166.6	0.008	0.980	2.64	1.383	0.986
Pb (II)	142.8	0.021	0.925	1.87	1.19	0.992

where K_2 is the constant of pseudo-second-order rate (g mg^{-1} min^{-1}), q_2 is the amount of metal ions adsorbed at equilibrium and q_t is the amount of metal ions adsorbed at any time. The equilibrium adsorption amount (q_2) and the pseudo-second-order rate parameters (K_2) can be given from the slope and intercept of plot of t/q_t versus t. The fitting results obtained from different models are summarized in Table II. Figure 11 shows the kinetic results of target ions adsorbed onto PBA-MNPs. The highest correlation coefficient for Cu (II) and Pb (II) are 0.994 and 0.998, respectively, indicating that pseudo-second-order model provides an excellent correlation for the adsorption of Cu (II) and Pb (II) ions on PBA-MNPs. Hence, the results stated that the chemical adsorption was the rate-limiting step involving the strong surface complexation between metal ions and the metal-binding groups on the surface of PBA-MNPs. In the kinetic study, the plots of adsorption capacity (q_t) against contact time (t) for the pseudo-second-order model are shown in Figure 12. The fits of the experimental results show that the pseudo-second-order model fit the data for the sorption of Cu (II) and Pb (II) ions very well. Therefore it is further illustrated that the rate of heavy metal ions sorption process is controlled by the chemical process.

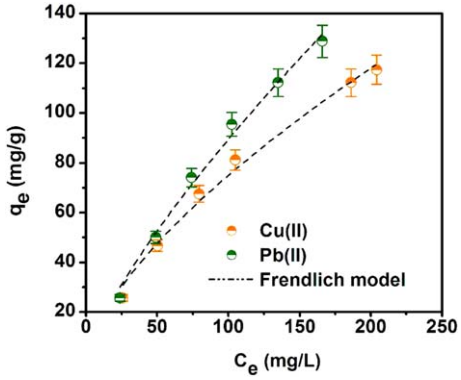

Figure 10. Isotherms for the sorption of Cu (II) and Pb (II) ions using PBA-MNPs. [Color figure can be viewed in the online issue, which is available at wileyonlinelibrary.com.]

Regeneration and Reuse of the PBA-MNPs Composite

The magnetic property of the magnetic nanocomposites provides recyclable adsorption performances. In order to recover the metal binding property, the desorption studies of the adsorbed Cu (II) and Pb (II) ions from PBA-MNPs were carried out by 0.1*M* HCl solution at 30°C. Desorption percentage was calculated as follows[57]:

$$\text{Desorption efficiency } (\%) = \frac{C_e^1 V}{qm} \times 100\%$$

where q is the adsorption capacity (mg/g), m is the mass of the adsorbent (mg), V is the volume of the aqueous solution (mL), C_e^1 is the concentration of metal ions aqueous solutions after desorbed from the adsorbent. A sample of 50 mg of PBA-MNPs adsorbed with Cu (II) and Pb (II) ions was added in the 15 mL 0.1*M* hydrochloric acid solution then shaken at 150 rpm using thermostat water bath for 5 h. Recycling adsorption/desorption experiments were repeated three times to establish the reusability of the adsorbents. As shown in Figure 13, the PBA-MNPs showed above 87.1% for Cu (II) and 82.69% for Pb (II) ions desorption efficiency after the three regeneration cycle process.

Table II. Kinetic Adsorption Parameters Obtained Using Pseudo-First-Order and Pseudo-Second-Order Models for the Adsorption of Cu (II) and Pb (II) Ions onto the PBA-MNPs

	Pseudo-first order			Pseudo-second order		
	q_e (mg/g)	K_1	R^2	q_e (mg/g)	K_2	R^2
Cu (II)	18.3	0.01	0.978	45.4	0.002	0.994
Pb (II)	12.8	0.011	0.912	50	0.005	0.998

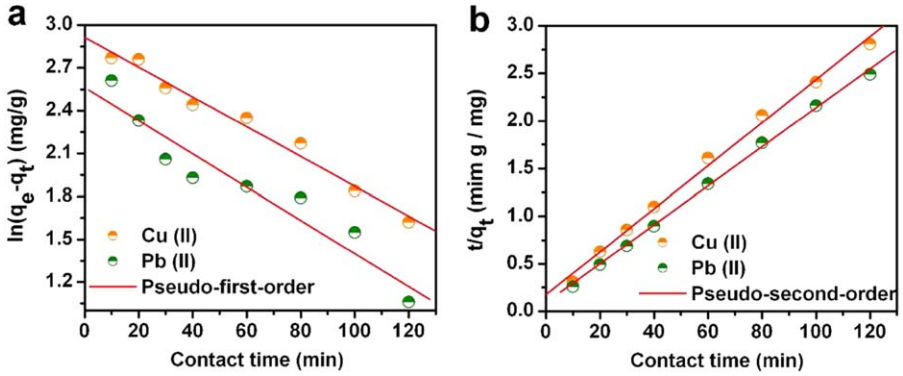

Figure 11. (a) Pseudo-first-order and (b) pseudo-second-order kinetic adsorption of Cu (II) and Pb (II) onto the PBA-MNPs. The test was performed at a pH value of 6 and 30°C. The initial concentration of the target ions was 100 mg/L. [Color figure can be viewed in the online issue, which is available at wileyonlinelibrary.com.]

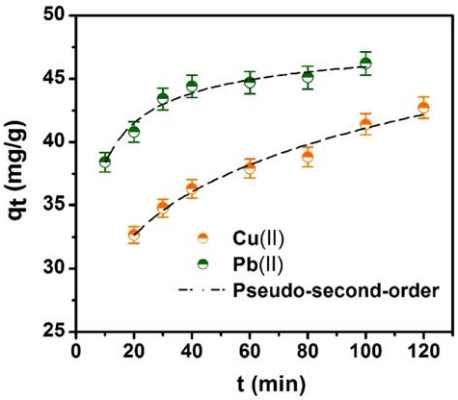

Figure 12. Plots of adsorption capacity versus time for Cu (II) and Pb (II) ions onto PBA-MNPs. [Color figure can be viewed in the online issue, which is available at wileyonlinelibrary.com.]

CONCLUSION

Poly(BA) functionalized magnetic nanoparticles were prepared via a simple chemical oxidation polymerization process and used as adsorbents for removal of heavy metal ions. The prepared products were a sphere-shaped nanostructure with magnetic properties of 7.5 emu g^{-1}, which make the magnetic nanocomposites recyclable for adsorption application. The adsorption capacity was strongly dependent on initial metal ions concentration, adsorption contact time, pH value, and adsorbent dose. The as-prepared PBA-MNPs showed that the maximum sorption capacities by applying the Langmuir equation were calculated to be 166.6 mg/g for Cu (II) ions and 142.8 mg/g for Pb (II) ions. The sorption isotherm is fitted better by the Freundlich model than by the Langmuir model, suggesting that sorption of metal ions on PBA-MNPs is heterogeneous adsorption. The pseudo-second-order model fitted the adsorption kinetic process of Cu (II) and Pb (II) on PBA-MNPs, indicating the chemical adsorption was the rate-limiting step. A recycle adsorption/desorption test revealed that PBA-MNPs can maintain the great adsorptive performance after three recycle experiments.

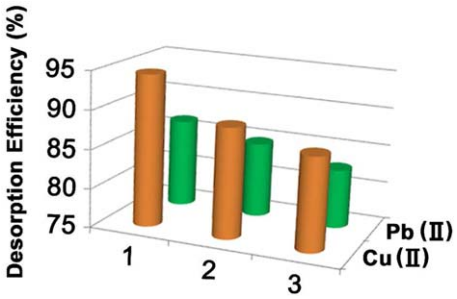

Figure 13. Desorption efficiency of Cu (II) and Pb (II) metal ions in serial recycle tests by the PBA-MNPs composite. (Cycle numbers: 1, 2, and 3). [Color figure can be viewed in the online issue, which is available at wileyonlinelibrary.com.]

ACKNOWLEDGMENTS

This work was supported by the Mineral and Ore Resources Comprehensive Utilization of Advanced Technology Popularization and Practical Research (MORCUATPPR) funded by China Geological Survey (Grant No. 12120113088300).

REFERENCES

1. Dong, A. L. D. E. T.; Sun, Y.; Lan, S.; Wang, Q.; Cai, Q.; Qi, X. Z.; Zhang, Y. L.; Gao, G.; Liu, F. Q.; Harnoode, C. K. *ACS Appl. Mater. Interfaces* **2013**, *5*, 8125.
2. Dorofeeva, E. O.; Elinson, M. N.; Vereshchagin, A. N.; Stepanov, N. O.; Bushmarinov, I. S.; Belyakov, P. A.; Sokolova O. O.; Nikishin, G. I. *RSC Adv.* **2012**, *2*, 4444.
3. Madadrang, C. J.; Kim, H. Y.; Gao, G. H.; Wang, N.; Zhu, J.; Feng, H.; Gorring, M.; Kasner, M. L.; Hou, S. F. *ACS Appl. Mater. Interfaces* **2012**, *4*, 1186.
4. Chen, Y. X.; Zhong, B. H.; Fang, W. M. *J. Appl. Polym. Sci.* **2012**, *124*, 5010.
5. Li, Y.; Wang, J. D.; Wang, X. J.; Wang, J. F. *Ind. Eng. Chem. Res.* **2012**, *51*, 6520.
6. Zhan, Y. C.; Luo, X. B.; Nie, S. S.; Huang, Y. N.; Tu, X. M.; Luo, S. L. *Ind. Eng. Chem. Res.* **2011**, *50*, 6355.

7. Jiang, J.; Xu, R. K.; Li, S. Z. *J. Chem. Eng. Data* **2010**, *55*, 5547.
8. Zhang, S.; Xu, F.; Wang, Y. F.; Zhang, W. Z.; Peng, X. L.; Pape, F. *Chem. Eng. J.* **2013**, *234*, 33.
9. Zhao, F. P.; Repo, E.; Yin, D. L.; Sillanpää, M. E. T. *J. Colloid Interface Sci.* **2013**, *409*, 174.
10. Bernardo, M.; Mendes, S.; Lapa, N.; Gonçalves, M.; Mendes, B.; Pinto, F.; Lopes, H.; Fonseca, I. *J. Colloid Interface Sci.* **2013**, *409*, 158.
11. Hasan, A. *J. Colloid Sci. Biotechnol.* **2013**, *2*, 153.
12. Rahman, M. M.; Elaissari, A. *J. Colloid Sci. Biotechnol.* **2012**, *1*, 3.
13. Elamssari, A.; Rodrigue, M.; Meunier, F.; Herve, C. *J. Magn. Magn. Mater.* **2001**, *225*, 127.
14. Roveimiab, Z.; Mahdavian, A. R.; Biazar, E.; Heidari, K. S. *J. Colloid Sci. Biotechnol.* **2012**, *1*, 82.
15. Chaabouni, A.; Marzougui, Z.; Elleuch, B.; Eissa, M. M.; Elaissari, A. *Sci. Adv. Mater.* **2013**, *5*, 854.
16. Deng, Y.; Wang, L.; Yang, W.; Fu, S.; Elaïssari, A. *J. Magn. Magn. Mater.* **2003**, *257*, 69.
17. Hasan, A. *J. Colloid Sci. Biotechnol.* **2013**, *2*, 155.
18. Montagne, F.; Mondain-Monval, O.; Pichot, C.; Elaissari A. *J. Polym. Sci. Part A: Polym. Chem.* **2006**, *44*, 2642.
19. Song, J.; Kong, H.; Jang, J. *J. Colloid Interface Sci.* **2011**, *359*, 505.
20. Wang, Y.; He, J.; Chen, J. W.; Ren, L. B.; Jiang, B. W.; Zhao, J. *ACS Appl. Mater. Interfaces* **2012**, *4*, 2735.
21. Xu, C. G.; Uddin, K. M. A.; Shen, X. T.; Jayawardena, H. S. N.; Yan, M. D.; Ye, L. *ACS Appl. Mater. Interfaces* **2013**, *5*, 5208.
22. Liu, X. Q.; Guan, Y. P.; Ma, Z. Y.; Liu, H. Z. *Langmuir* **2004**, *20*, 10278.
23. Kong, H.; Song, J.; Jang, J. *Chem. Commun.* **2010**, *46*, 6735.
24. Roy, A.; Chakraborty, S.; Kundu, S. P.; Adhikari, B.; Majumder, S. B. *J. Appl. Polym. Sci.* **2013**, *129*, 15.
25. Wang, L.; Li, Y. H.; Han, Z. D.; Chen, L.; Qian, B.; Jiang, X. F.; Pinto, J.; Yang, G. *J. Mater. Chem. A* **2013**, *1*, 8385.
26. Gulce, H. D.; Eskizeybek, V.; Haspulat, B.; Sarı, F.; Gulce, A.; Avcı A. *Ind. Eng. Chem. Res.* **2013**, *52*, 10924.
27. Ali, S. D.; Hussain, S. T.; Gilani, S. R. *Appl. Surf. Sci.* **2013**, *271*, 118.
28. Rana, V. K.; Selvaraj, M.; Parambadath, S.; Chu, S. W.; Park, S. S.; Mishra, S.; Singh, R. P.; Ha, C. S. *J. Solid State Chem.* **2012**, *194*, 392.
29. Chen, Z. B.; Sun, Y. Y. *Ind. Eng. Chem. Res.* **2006**, *45*, 2634.
30. Ma, Y. R.; Zhang, X. L.; Zeng, T.; Cao, D.; Zhou, Z.; Li, W. H.; Niu, H. Y.; Cai, Y. Q. *ACS Appl. Mater. Interfaces* **2013**, *5*, 1024.
31. Zhao, C. J.; Chou, S. L.; Wang, Y. X.; Zhou, C. F.; Liu, H. K.; Dou, S. X. *RSC Adv.* **2013**, *3*, 16597.
32. Yang, C. L.; Guan, Y. P.; Xing, J. M.; Liu, H. Z. *Langmuir* **2008**, *24*, 9006.
33. Jia, Y.; Luo, T.; Yu, X. Y.; Sun, B.; J. Liu, H.; Huang, X. J. *RSC Adv.* **2013**, *3*, 15805.
34. Zhou, L.; He, B. Z.; Huang, J. C. *ACS Appl. Mater. Interfaces* **2013**, *5*, 8678.
35. Ishpala, O. S P.; Kumar, M.; Kumara, S. *Appl. Surf. Sci.* **2010**, *256*, 7371.
36. Zhang, Y. T.; Li, L. L.; Ma, W. F.; Zhang, Y.; Yu, M.; Guo; J.; Lu, H. J.; Wang, C. C. *ACS Appl. Mater. Interfaces* **2013**, *5*, 614.
37. Yi, D. K.; Lee, S. S.; Papaefthymiou, G. C.; Ying, J.Y. *Chem. Mater.* **2006**, *18*, 614.
38. Leng, C. J.; Wei, J. H.; Liu, Z. Y.; Xiong, R.; Pan, C. X.; Shi J. *J. Nanopart Res.* **2013**, *15*, 1643.
39. Chiu, W.; Khiew, P.; Cloke, M.; Isa, D.; Lim, H.; Tan, T.; Huang, N.; Radiman, S.; Abd-Shukor, R.; Hamid, M. A. A.; Chia, C. *J. Phys. Chem. C.* **2010**, *114*, 8212.
40. Razmjou, A.; Barati, M. R.; Simon, G. P.; Suzuki, K.; Wang, H. T. *Environ. Sci. Technol.* **2013**, *47*, 6297.
41. Zhong, W.; Liu, P.; Tang, Z. B.; Wu, X. L.; Qiu, J. H. *Ind. Eng. Chem. Res.* **2012**, *51*, 12017.
42. Ren, Y.; Abbood, H. A.; He, F. B.; Peng, H.; Huang, K. X. *Chem. Eng. J.* **2013**, *226*, 300.
43. Sitko, R.; Turek, E.; Zawisza, B.; Malicka, E.; Talik, E.; Heimann, J.; Gagor, A.; Feist, B.; Wrzalikb, R. *Dalton Trans.* **2013**, *42*, 5682.
44. Rao, R. A. K.; Ikram, S. *Desalination* **2011**, *277*, 390.
45. Thirumavalavan, M.; Lai, Y.-L.; Lin, L.-C.; Lee, J.-F. *J. Chem. Eng. Data* **2010**, *55*, 1186.
46. Mahapatra, A.; Mishra, B. G.; Hota, G. *J. Hazard. Mater.* **2013**, *258–259*, 116.
47. Karami, H. *Chem. Eng. J.* **2013**, *219*, 209.
48. Powell, K. J.; Brown, P. L.; Byrne, R. H.; Gajda, T.; Hefter, G.; Sjöberg, S.; Wanner, H. *Pure Appl. Chem.* **2007**, *79*, 895.
49. Powell, K. J.; Brown, P. L.; Byrne, R. H.; Gajda, T.; Hefter, G.; Leuz, A. K.; Sjöberg, S.; Wanner, H. *Pure Appl. Chem.* **2009**, *81*, 2425.
50. Powell, K. J.; Brown, P. L.; Byrne, R. H.; Gajda, T.; Hefter, G.; Leuz, A. K.; Sjöberg, S.; Wanner, H. *Pure Appl. Chem.* **2011**, *83*, 1163.
51. Takafuji, M.; Ide, S.; Ihara, H.; Xu, Z. H. *Chem. Mater.* **2004**, *16*, 1977.
52. Tang, R.-R.; Gu, G.-L.; Zhao, Q. *Spectrochim. Acta A* **2008**, *71*, 371.
53. Zhou, J.; Wang, L.-F.; Wang, J.-Y.; Tang, N. *J. Inorg. Biochem.* **2001**, *83*, 41.
54. Huang, J.; Ye, M.; Qu, Y. Q.; Chu, L. F.; Chen, R.; He, Q. Z.; Xu, D. F. *J. Colloid Interface Sci.* **2012**, *385*, 137.
55. Abraham, T. N.; Kumar, R.; Misra, R. K.; Jain, S. K. *J. Appl. Polym. Sci.* **2012**, *15*, 670.
56. Mahmoud, H. R.; EI-Molla, S. A.; Saif, M. *Powder Technol.* **2013**, *249*, 225.
57. Liu, L.; Liu, S. X.; Zhang, Q. P.; Li, C.; Bao, C. L.; Liu, X. T.; Xiao, P. F. *J. Chem. Eng. Data* **2013**, *58*, 209.